Near-source effects and non-linear Site Response at Kashiwazaki-Kariwa Nuclear Power Plant, in the 2007 Chuetsu-Oki Earthquake: evidence from surface and downhole records and 1D numerical simulations

Filippo Gatti, Fernando Lopez-Caballero, Roberto Paolucci, Didier Clouteau

Near-source effects and non-linear site response at Kashiwazaki-Kariwa Nuclear Power Plant, in the 2007 Chuetsu-Oki earthquake: evidence from surface and downhole records and 1D numerical simulations

Filippo Gatti[1,2] · Fernando Lopez-Caballero[1] · Roberto Paolucci[2] · Didier Clouteau[1]

Abstract The aim of this paper is to clarify the extent of near-source effects and non-linear soil response that took place at the Japanese nuclear site of Kashiwazaki-Kariwa, during the M_W 6.6 *Niigata-Ken Chūetsu-Oki* earthquake (July, 16th 2007). The interest of this case study stems from the relative small source-to-site distance and shallow hypocenter depth, coupled with the consistent seismic record database available from two down-hole arrays of strong motion accelerometers, installed within the nuclear site. Records were processed first to highlight those features related to near-source conditions, such as directivity and polarization, and, subsequently, to identify dependence of site response on the direction of motion and on the non-linear soil behaviour. Moreover, borehole interferometry was used to check the two available velocity profiles (estimated by in situ PS logging) used for 1D linear equivalent numerical simulations. In one case, an improved agreement with the empirical amplification functions was obtained using a smoothed profile. The main non-linear features highlighted by signal processing were globally reproduced by means of linear-equivalent analyses, that pointed out the strong influence of the input motion direction. Among the principal results of this research, it was found that the hanging-wall and directivity effects along with the non-linear site-effects

✉ Filippo Gatti
filippo.gatti@centralesupelec.fr

Fernando Lopez-Caballero
fernando.lopez-caballero@centralesupelec.fr

Roberto Paolucci
roberto.paolucci@polimi.it

Didier Clouteau
didier.clouteau@centralesupelec.fr

[1] Laboratoire de Mécanique des Sols, Structures et Matériaux CNRS UMR 8579, CentraleSupélec - Université Paris-Saclay, 8-10 Rue Joliot Curie, 91190 Gif-Sur-Yvette, France

[2] Dipartimento di Ingegneria Civile e Ambientale, Politecnico di Milano, P.zza Leonardo da Vinci 32, 20133 Milan, Italy

dominate the ground response during the main shock, and that the site amplification features are strongly dependent on the rotation angle of the horizontal components.

Keywords Non-linear seismic site response · Near-source ground motion · Seismic interferometry

1 Introduction

Seismic site effects represent the modification (in amplitude, direction and frequency content) that the shallow geological layers induce on the radiated wave field while travelling from the nucleation point on the seismic fault to the considered site. In the last few decades, complex 3D non-linear site-effects have been extensively observed and studied (e.g. during the 1985 Mexico City, 1994 Northridge, 1995 Hyogoken-Nanbu (Kobe) and the more recent 2011 Tōhoku earthquake). Local soil conditions within the upper part of the Earth's crust play a crucial role in the seismic design of building's foundation, since they dramatically increase the destructive power of seismic ground motion on structural components (Faccioli and Vanini 2003; Regnier et al. 2013). Namely, the main features to be assessed are (1) the (de-) amplification due to soil layering, (2) the scattering caused by interactions with geological interfaces and topographical surfaces, (3) the time-dependent non-linear stiffness decay of geomaterials, triggered at relatively small strain magnitudes (Hashash and Groholski 2010). In near-source conditions, uncertain faulting mechanisms and propagation path add further complexity to the problem. In such a case, addressing seismic hazard evaluation should be re-examined carefully, especially when dealing with critical structures as nuclear power plants.

In this context, strong ground motion recordings represent a great source of information to calibrate numerical models for site-specific seismic response analyses. For this purpose, arrays of seismometers deployed down-hole, till the depth of the *engineering bedrock*, provide an additional relevant evidence on the effect of shallow geology on the seismic motion. Signal processing techniques unravel the non-linear evolution of soil properties, as well as some major features of ground motion in near-source conditions (e.g. the possible impulsive nature of velocity records). Nevertheless, the exploitation of record databases is not always straight-forward and the interpretation of results can be difficult.

In this paper, borehole recordings were processed to characterize the seismic site effects observed during the M_W6.6–M_{JMA}6.8 *Niigata-Ken Chūetsu-Oki* (NCO) earthquake, occurred on July, 16th 2007 (10:13 UCT) off the coast of the Niigata prefecture (Japan). The NCO earthquake affected an area of approximately 100 km of radius along the coastal line of South-West Niigata prefecture, till a maximum depth of 17 km (Pavlenko and Irikura 2012). The seismic sequence caused the shut-down of the Kashiwazaki-Kariwa Nuclear Power Plant (KK-NPP), located close to the epicenter location (see Fig. 1).

The plant consists of seven generators (see map in Fig. 2) and it is located on the hanging wall of the mentioned fault, above a region of relatively high slip (Ozawa 2008). The strong motion sensors indicated that during the main shock the site experienced nearly twice the peak ground acceleration (PGA) considered in the plant design. Moreover, the rather high variability of PGA values within the site area is representative of directivity features of the source radiation. Pavlenko and Irikura (2012) made an extensive study to assess the non-linear site response at KK-NPP. They performed one-dimensional analyses on representative soil columns, estimating that the reduction of the shear moduli in the upper softer layers was about 30–35% during the main shock and about 1.5–3% during the

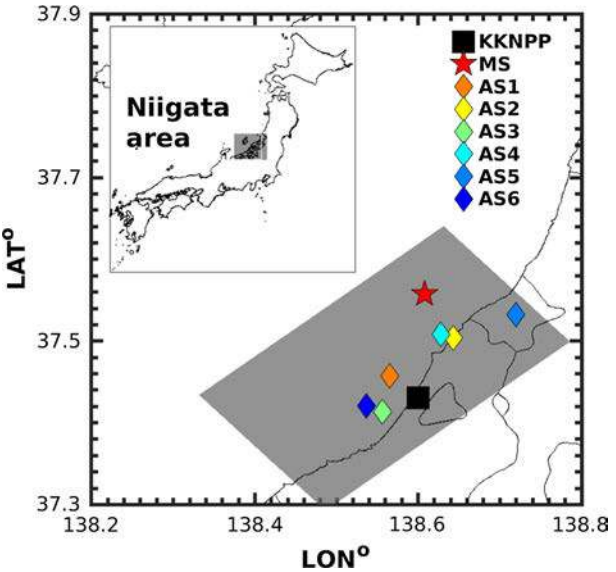

Fig. 1 Map of the area in the surroundings of the KK-NPP. Epicenters of main shock (MS) and selected aftershocks (AS) are depicted; the grey shaded area represents the fault projection. Small axes: map of west Japan highlighting the region of Niigata

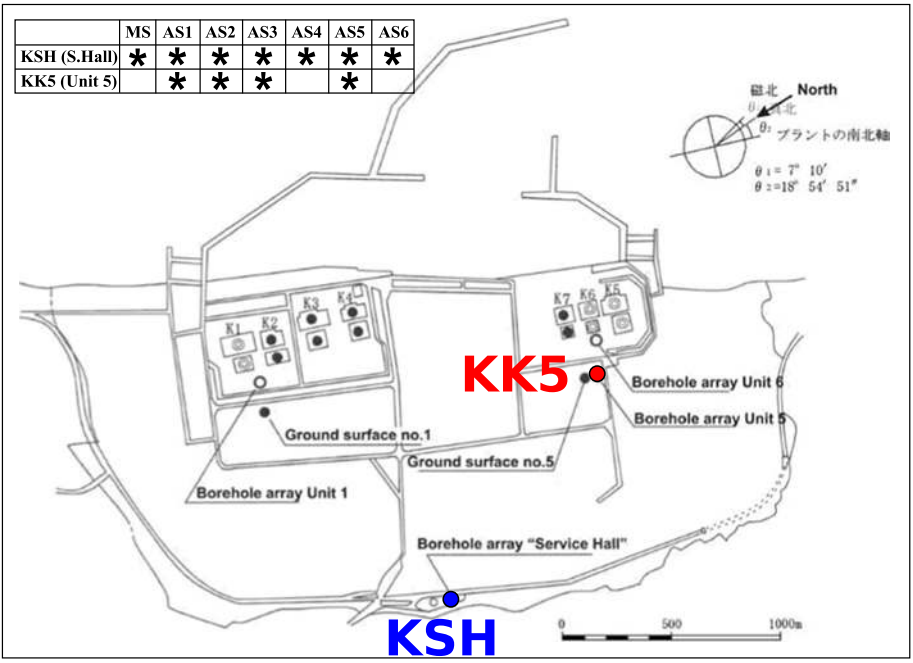

Fig. 2 Geo-referenced and scaled map of the Kashiwazaki-Kariwa Nuclear Power Plant (courtesy of TEPCO 2008). Down-hole arrays considered in this work are located at the Service Hall (KSH) and Unit 5 (KK5), about 1 km distant. Table on the top-left corner denotes the events for which records are available

aftershocks. Another extensive work on the seismic characterization of the Kashiwazaki-Kariwa Nuclear Power Plant during the NCO earthquake was performed by Yee et al. (2011). The authors focused on the simulation of site response recorded free-field at the Service Hall (KSH). They compared equivalent linear and full non-linear soil column models, adjusting input parameters according to in situ and laboratory tests on soil samples from KK-NPP, in an extensive study which encompasses a liquefaction analysis.

The aim of the paper is threefold: (a) to track the seismic wave path and to outline the site response dependency on the direction of motion in particular under near field conditions; (b) to compare and discuss the V_s profiles estimated by in situ PS logging with the analysis of the down-hole records from the borehole recordings applying interferometry technique; and (c) to study the main non-linear features at the site by signal processing. Moreover, this study assesses some of the features of near-source ground motion and it describes the variability of seismic response within the KK-NPP. To this end, some representative locations were selected, with a significant quantity of high-quality seismic records available, to test the applicability and the performance of standard numerical approaches, consisting of 1D soil column models analyzed within the equivalent linear assumption. This is a crucial step before any further 3D model involving complicated surface geology and faulting mechanism. In Sect. 2 a general overview of the main features of the incident wave motion is presented, by proving its quasi-vertical propagation as well as its impulsive nature (symptomatic of near-fault conditions). Besides, some insight is presented on both recorded directivity effects and on the borehole-to-surface amplification. In Sect. 3, the estimated layered geological configuration is checked by means of seismic interferometry, a technique suitable to assess the non-linear evolution of values during shock. Finally, in Sect. 4 the results obtained via equivalent linear analyses on 1D soil columns are compared to the recorded response, for both the aftershock and the main shock.

2 Overview on seismic site response at KK-NPP

2.1 Introduction to recorded ground motion at KK-NPP during the NCO mainshock

The NCO earthquake occurred as a result of a buried reverse-slip motion nucleated at the estimated hypocenter depth of 8 km and causing no significant surface rupture (Aochi et al. 2013). The distance of the nuclear site of Kashiwazaki-Kariwa to the surface projection of the fault (i.e. Joyner–Boore distance) is $R_{JB} = 0$ km, whereas the rupture distance is $R_{RUP} = 16$ km (Yee et al. 2011).

Despite the dense observation network in operation at the time (considering Kik-Net records as well) and the extensive number of seismological studies, the faulting mechanism remains uncertain (see for instance Aoi et al. 2014; Kato et al. 2008). By the time of the 2007 NCO earthquake, KK-NPP was instrumented with an older and a more recent systems of accelerometers. The horizontal recording devices (EW and NS respectively) are oriented with respect to the Plant North (see Fig. 2). The *Tokyo Electric Power Company* (TEPCO) provided the azimuthal deviation of some seismometers due to their installation down-hole. Ground motion at 33 locations were registered by the new system, although the recordings of the old system obtained at other 66 locations (including two free-field down-hole arrays and most structural arrays) were lost with the exception of the peak values (Kayen et al.

Table 1 List of the PGA values at KK-NPP during the NCO main-shock (IAEA 2014). Seismometers deployed at the Service Hall recorded the whole main shock time-history and most of the aftershock cluster. All the other devices belong to the most recent array installed at KK-NPP

Observation point		PGA (cm/s^2)		
		NS	EW	UD
Service Hall				
Free-field				
SG1	T.M.S.L. + 65.1 m	347	437	590
SG2	T.M.S.L. + 16.7 m	340	411	179
SG3	T.M.S.L − 31.9 m	403	647	174
SG4	T.M.S.L − 182.3 m	430	728	160
Ground surface				
Unit 1				
1-G1	Rec. Shed-Reactor 1	890	890	715
Unit 5				
5-G1	Rec. Shed-Reactor 5	964	1223	539
Unit 1				
Reactor				
1-R1	2nd floor	599	884	394
1-R2	Basement 5	311	680	408
Turbine				
1-T2	1st floor-pedestal	1862	1459	741
Unit 2				
Reactor				
2-R1	2nd floor	517	718	412
2-R2	Basement 5	304	606	282
Turbine				
2-T1	1st floor	431	764	594
2-T2	1st floor-pedestal	642	1159	650
2-T3	Basement 3	387	681	470
Unit 3				
Reactor				
3-R1	2nd floor	525	650	518
3-R2	Basement 5	308	384	311
Turbine				
3-T2	1st floor-pedestal	1350	2058	619
3-T3	Basement 3	581	549	513
Unit 4				
Reactor				
4-R1	2nd floor	606	713	548
4-R2	Basement 5	310	492	337
Turbine				
4-T1	1st floor	411	560	549
4-T2	1st floor-pedestal	614	763	526
4-T3	Basement 3	348	442	443

Table 1 continued

Observation point		PGA (cm/s^2)		
		NS	EW	UD
Unit 5				
Reactor				
5-R1	3rd floor	472	697	331
5-R2	Basement 4	277	442	205
Turbine				
5-T2	2nd floor-pedestal	1166	1157	533
Unit 6				
Reactor				
6-R1	3rd floor	554	545	578
6-R2	Basement 3	271	322	488
Unit 7				
Reactor				
7-R1	3rd floor	367	435	464
7-R2	Basement 3	267	356	355
Turbine				
7-T1	2nd floor	418	506	342
7-T2	2nd floor-pedestal	673	1007	362
7-T3	Basement 2	318	322	336

T.M.S.L. Tokyo Mean Sea Level

2009). Table 1 summarizes the PGA recorded at each location within the KK-NPP during the main shock. The largest peak ground acceleration at free field surface in the horizontal direction was 1.25 g (EW), as measured at the seismic observation shed for Unit 5 (5-G1). In the vertical direction it was 0.73 g, as measured at the seismic observation shed for Unit 1 (1-G1). Recorded accelerations reached up to 0.69 g (EW) at the basement of Unit 1, largely above the design specification for safe shutdown, i.e. 0.46 g, and well above the rapid restart specification for key equipment in the plant, i.e. 0.28 g. At the reactor basements of Unit 2, 3 and 4 (located on the southwest part of the plant), PGAs were those recorded at Unit 5, 6 and 7 (located on the northeast part of the site) (Pavlenko and Irikura 2012). Figure 3 portrays the recorded acceleration time-histories at three different locations free-field (SG1, G.L. − 2.4 m, located at the Service Hall; 1G1, G.L. 0 m, located at the shed of the Unit 1 reactor; 5G1, G.L. 0 m, located at the shed of Unit 5 reactor).

Figure 4 shows the recorded pseudo-acceleration response (*Sa*) at the same locations, compared to the design response spectrum at Ground Surface JDC-2000, computed according to Midorikawa et al. (2004), based on the notification of the Japanese Ministry of Land, Infrastructure and Transport (2000). The recorded spectral response exceeded at 5G1 and 1G1 (Fig. 4b, c) the Japanese input design spectrum for an earthquake with a return period of 500 years. As confirmed by many authors (Kokusho and Suzuki 2008, among others), the recorded ground motion entailed a rather amplified low period component, which exceeded the design response. However, at the Service Hall, large ground strains

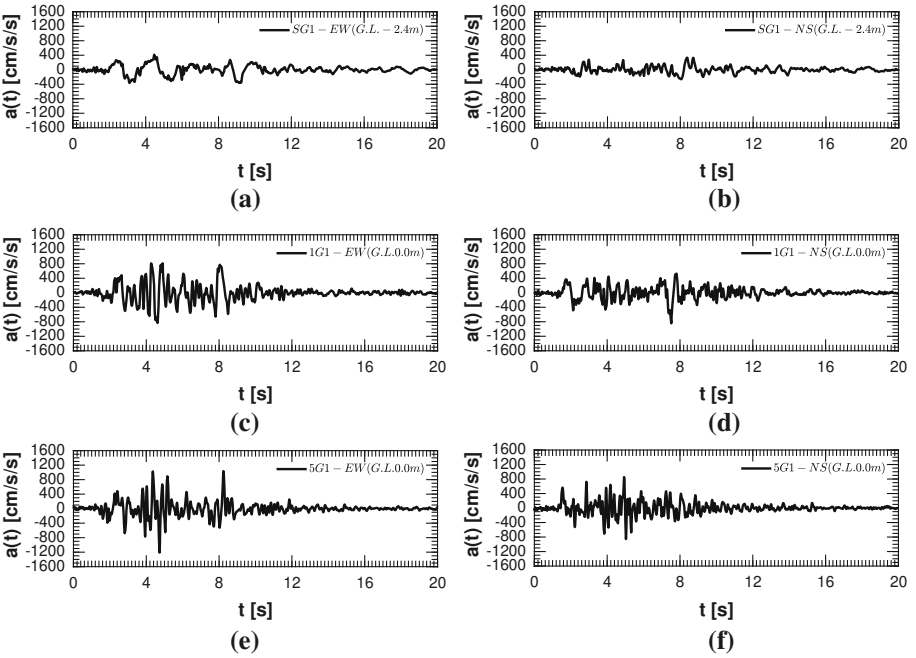

Fig. 3 Acceleration time-histories recorded at **a**, **b** SG1 (G.L. − 2.4 m, along the array KSH, at the KKNPP Service Hall, free-field), **c**, **d** 1G1 (G.L. 0 m, belonging to the Unit 1 shed) and **e**, **f** 5G1 (G.L. 0 m, belonging to the Unit 5 shed)

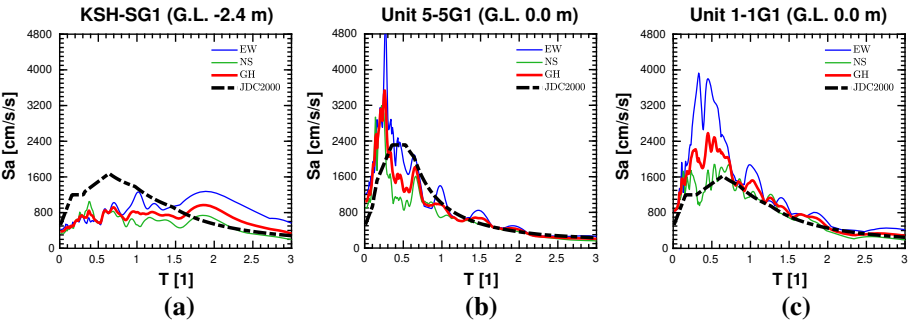

Fig. 4 Pseudo-acceleration response spectrum *Sa* recorded at **a** SG1 (G.L. − 2.4 m, along the array KSH, at the KKNPP Service Hall, free-field), **b** 5G1 (G.L. 0 m, belonging to the Unit 5 shed) and **c** 1G1 (G.L. 0 m, belonging to the Unit 1 shed). Blue and green lines refer to the recorded response spectra during the NCO main shock, along the EW and NS direction respectively, while red spectra represent their geometric mean. Black dashed line refers to the design spectrum proposed by the Japanese building code (2000), and computed according to Midorikawa et al. (2004)

were estimated, entailing a consistent non-linear site effect. This resulted into a de-amplification of the wave motion at ground surface, as proved by the short-period spectral ordinates recorded at SG1 (Fig. 4a), lower than the other sites considered.

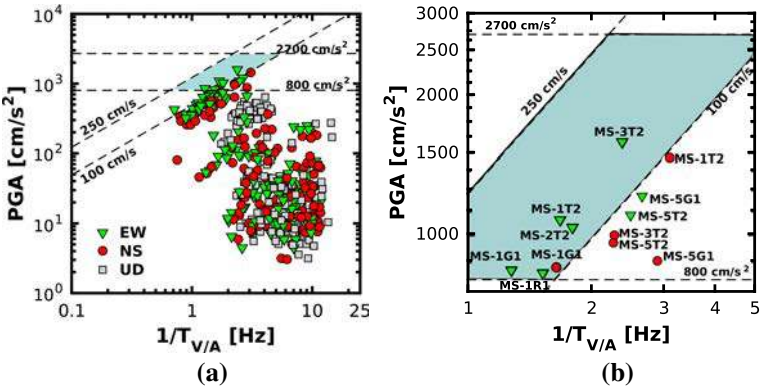

Fig. 5 PGA values with respect to the inverse of the *equivalent harmonic dominant period* $1/T_{V/A}$ for all the record database provided by TEPCO. **a** All the values in the two directions (EW-NS), **b** zoom on the area delimited by the dashed lines representing the PGA-PGV limit values and suggested by Kawase (2011), after Kobe earthquake

To throw light on the relationship between recorded ground motion with its potential to produce severe structural damage, Fig. 5 highlights the relationship between the PGA and the inverse of the *predominant harmonic period* $1/T_{V/A}$, estimated as follows (Green and Cameron 2003; Kawase 2011):

$$\frac{1}{T_{V/A}} = \frac{\alpha^{PGA}_{(\xi=5\%)}}{\alpha^{PGV}_{(\xi=5\%)}} \frac{PGA}{2\pi PGV} \tag{1}$$

Equation (1) is based on the assumption that ground motion is dominated by the harmonic component corresponding to the intersection between the constant spectral acceleration and velocity regions of a 5% damped Newmark–Hall type spectrum constructed using the actual PGA–PGV values (Green and Cameron 2003). In this sense, $\alpha^{PGV}_{(\xi=5\%)}$ and $\alpha^{PGA}_{(\xi=5\%)}$ are the median spectral amplification factors for horizontal motion proposed by Newmark and Hall (1982) for the constant velocity and constant acceleration regions of 5% damped response spectra. Green and Cameron (2003) suggest values of $\alpha^{PGA}_{(\xi=5\%)} = 2.12$ and $\alpha^{PGV}_{(\xi=5\%)} = 1.65$.

Black dashed lines in Fig. 5 represent respectively iso-PGA (i.e. 800–2700 cm/s^2) and iso-PGV lines (i.e. 100–250 cm/s), the latter with a slope from left-down side to right-up side. Based on the observations in 1995 Kobe earthquake, those lines delimit the region above which major damages are expected (Kawase 2011), and roughly correspond, according to the relationship between the Modified Mercalli Intensity (IMM) and PGV/PGA values proposed by Wald et al. (1999), to IMM X. As shown in Fig. 5b, a few points range within the polygonal area included between the mentioned black dashed lines. Such points refer to the main shock (MS) and to devices placed on (1) the turbines at the basement level (1T2, 2T2 and 3T2, on turbines at Units 1, 2 and 3 respectively), (2) on the reactor of Unit 1 at first floor (1R1) and (3) at the ground surface nearby Unit 1 (point 1G1). Figure 4 is in agreement with the evidence highlighted by site inspections (see for example IAEA 2014), i.e. that the large ground deformations damaged Unit 3 (although with no particular safety significance).

2.2 Records considered in this study

Due to technical problems occurred during the NCO earthquake main shock, records from two free-field down-hole arrays and most structural arrays were lost, with the exception of the peak values (listed in Table 1). A single 4-device free-field array at the Service Hall (KSH) was recovered and provided a complete dataset, that was considered in this work to detect the variation with depth of earthquake ground motion during the main shock. In addition, the dataset recorded at Unit 5 (KK5) was considered, which, although having lost the main shock, provided a significant dataset during the aftershock sequence. Location of KSH and KK5 arrays is depicted in Fig. 2. The distance between the boreholes is relatively large (approximately 1 km) and the geology and topography quite complicated. PS-logging profiles were provided by TEPCO (see Fig. 6), as well as reference degradation curves for four different soil layers (where G_{max} and G are initial and secant shear moduli, γ the shear distortion and D the hysteretic damping).

In Table 2 the set of peak values (PGA and PGV) of the seismic sequence considered hereafter and recorded at the two mentioned downhole array is reported.

2.3 Directivity and *hanging wall* effects

Coupling $T_{V/A}$ and PGA as in Fig. 5 provides a significant and intuitive picture of the severity of the ground motion. However, in near-field conditions, large velocity pulse coupled with a corresponding large peak displacement considerably enhance the damage potential (Cox and Ashford 2002). Strong velocity pulses may exert an extreme demand on the structural components (e.g. Mavroeidis and Papageorgiou 2003; Mavroeidis et al. 2004; Luco and Cornell 2007). For this reason, several authors already argued on the pulse-like shape of some velocity time-histories recorded at KK-NPP. For instance, Uetake et al. 2008 observed three significant pulses at KSH array, possibly associated to the three major asperities identified on the fault plane, via waveform inversion. In this paper, the occurrence of velocity pulses at the KK-NPP was verified considering the borehole records available and by classifying them as according to the ranking criterion proposed by Baker (2007) (excluding late arrivals and small events).

Figure 7 schematically presents the results according to the Baker (2007) classification. The Pulse Indicator (PI) [see Eq. (2)] is based on two predictor variables: the peak ground velocity (PGV) of the residual record—obtained by subtracting the extracted pulse from the as-recorded time-history—divided by the original record's PGV (i.e. PGV-ratio, reported along the x-axis in Fig. 7b) and the energy of the residual record divided by the original record's energy (i.e. the Energy-ratio, reported along the y-axis in Fig. 7c and computed by dividing the Cumulative Squared Velocity (CSV) of the residuum by the original record's CSV).

$$PI = \frac{1}{1 + e^{-23.3+14.6PGV_{ratio}+20.5Energy_{ratio}}} \tag{2}$$

Late pulses were considered as outliers (criterion CT1), as well as pulses associated to PGV < 30 cm/s (criterion CT2). Records with PI scoring above 0.85 and below 0.15 were classified as pulses (red circles in Fig. 7b, c) and non-pulses respectively (green diamonds in Fig. 7b, c). The remaining time-histories were not classified since they do not comply the seismological criteria mentioned above (i.e. light-blue diamonds in Fig. 7b, c). In pulse identification, recorded components were rotated by 5 different angles to check the

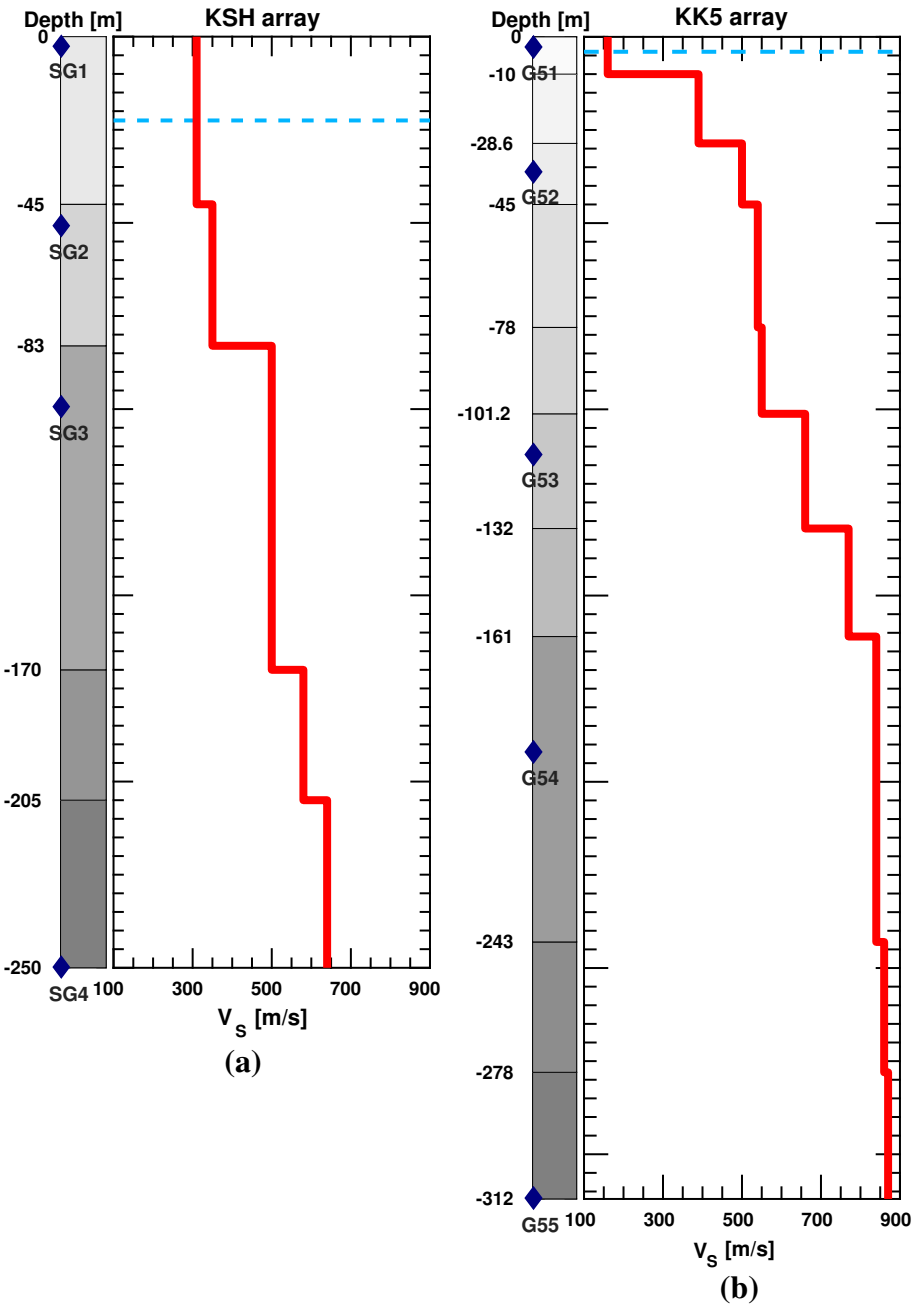

Fig. 6 V_S profiles and seismometers locations at **a** array KSH (Service Hall) and **b** KK5 (Unit 5)

preferential direction they mostly come from, with respect to fault normal (FN) and fault parallel (FP) directions, corresponding to 0° and 90° in Fig. 7c. In the latter, each point corresponds to the direction at which the greatest pulse-like wave form has been extracted.

Table 2 List of the earthquake considered in the paper

	M_{JMA}	R (km)	PGA-H (cm/s^2)		PGA-V (cm/s^2)		PGV-H (cm/s)		PGV-V (cm/s)	
			SG1	G51	SG1	G51	SG1	G51	SG1	G51
MS	6.8	16	433	–	583	–	123	–	44	–
AS1	3.7	5	36	23	42	20	1	1	0.7	0.4
AS2	5.8	10	189	275	188	88	25	22	9	4
AS3	4.2	4	50	42	36	23	2	2	0.8	0.4
AS4	4.4	10	70	–	65	–	2	–	1	–
AS5	4.8	17	77	101	50	27	5	5	2	1
AS6	3.2	6	34	–	26	–	1	–	0.5	–

M_{JMA} magnitude according to the Japanese Meteorological Agency, R represents the epicentral distance in km. PGA-H/-PGV-H and PGA-V/PGV-V represents the peak ground acceleration/velocity on the horizontal and vertical directions respectively. SG1 and G51 denote the surface stations of boreholes KSH and KK5 respectively. Not available values (due to data loss) are reported as –

The pulse-like wave field is not oriented along a preferential direction although most of the extracted pulses come from a + 30° angle with respect to the FN direction, approximately along the site-to-epicenter direction. Since KK-NPP is located on the fault hanging wall of a buried reverse-slip fault, wave pulses were also observed on the vertical component, although not shown here for brevity. High PGA values along the vertical direction are in agreement with the rapid uplift of the ground during the fault slip, caused by elastic rock rebound effects (Bolt 2004). This result is typical when forward directivity condition is met. Further studies on the so called *hanging wall effect* for this earthquake may be found in Spudich et al. (2013). Although the followed procedure does not discriminate the mechanism originating the pulse-like recordings, it helps in quantifying the near-field effects for engineering purposes, barely described by traditional tools (such as the pseudo-spectral acceleration response).

2.4 Polarization of the wave motion

When simplified 1D numerical simulations of seismic wave propagation are performed, the assumption is implicitly made that the input motion has a quasi-vertical incidence. To verify this assumption a polarization analysis of the records was carried out, consisting into a linear transformation of the three components of motions into the principal ones (e.g. vertical and radial/transverse projections with the respect to the source-to-site direction). In fact, those components are associated to the eigenvectors/values of the cross-correlation matrix (at zero lag time) between the three components. The azimuth angle AZ and the angle of apparent incidence IN (e.g. angle of deviation from the vertical) were estimated within a time-window sliding along the whole record duration. Those parameters define the wave trajectory along the whole duration of the records, considering time window of 0.1–0.5 s and low-pass filtering up to 2.5–5 Hz to get stable results. In Fig. 8 stereo-net projections summarize the average wave incidence computed at P-wave arrival time (northern axis refers to local KK-NPP's one).

Signals drift vertically towards the surface, as outlined by Gatti et al. (2015). Nevertheless, such rectilinear and vertical feature decays in time, due to small influence of

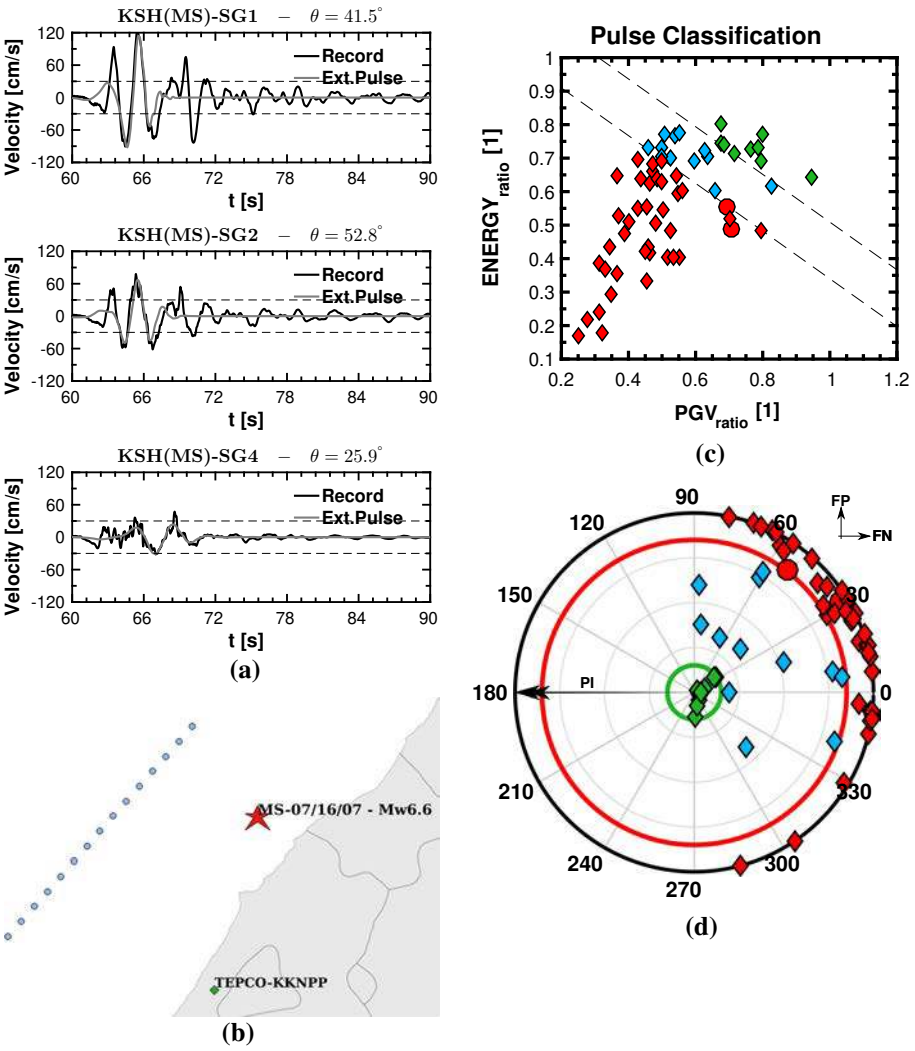

Fig. 7 Pulse classification for borehole records at KK-NPP (horizontal components). **a** Comparison between recorded velocity signals and extracted pulses, **b** map of the surrounding of the KK-NPP with the causative fault trace and NCO earthquake main shock, **c** pulse classification according to Energy-ratio and PGV-ratio. Red and green points represent respectively pulse-like and non-pulse-like signals, whereas light-blue points cannot be clearly classified automatically (according to predictor factor proposed by Baker 2007). Circles indicate the extracted pulse fulfills criteria CT1 and CT2 (mentioned in this paragraph), **d** polar plot portraying the angles at which pulses were extracted, with respect to the fault-normal (FN) and fault-parallel directions (FP). The angle corresponds to the one that provides the highest PI

spurious waves impinging the borehole at sub-horizontal incidence. Concerning the azimuth, it must be noted that the focal mechanism is still uncertain (Aochi et al. 2013), due to the difficulties to deconvolve the source mechanism from the effects of 3D geological structures. Moreover, two potential fault planes have been proposed so far: a NW dipping plane striking at 215° and a SE dipping one at 49° strike. Aftershock locations fell along both planes, although their majority was located along the SE dipping plane (strike 49°,

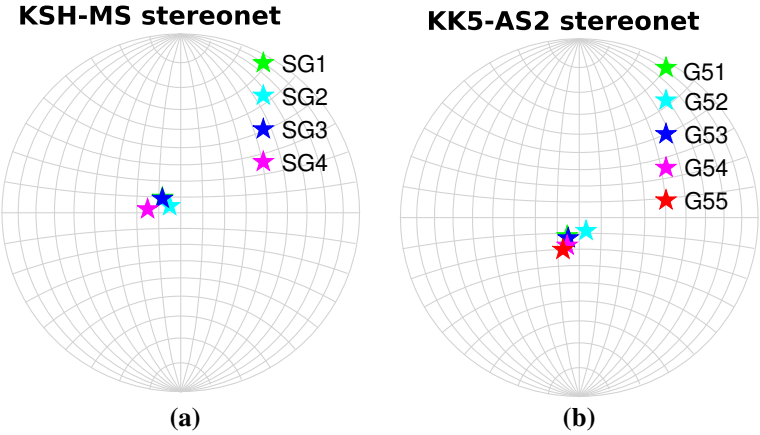

Fig. 8 a Stereo-net referring to main shock recorded at KSH, **b** stereo-net referring to aftershock 2 (the most intense) at KK5

Kayen et al. 2009; Aochi et al. 2013). Estimated azimuth values are coherent with the observed tectonic mechanisms.

Once vertical incidence has been proven, standard 1D soil column analyses may be carried out. For simplicity, it was assumed that they are made independently for each horizontal direction. Of course, this is strictly valid only for linear analyses, while it does not hold true for equivalent linear and nonlinear analyses, since the equivalent strain should be defined taking both components of motion acting at the same time, for example through the 2nd invariant of the deviatoric shear strain, factored by some quantity. To minimize such coupling effect, preferential direction of motions can be identified, e.g. the two components associated to maximum and minimum energy release. For instance, Penzien and Watabe (1975) defined the principal axes of ground motion as the directions along which the three components of motions are statistically independent. They assumed projected time series uncorrelated, although uncorrelated variables are not a priori statistically independent. Along the *major principal axis*, the motion amplitude, measured for instance as Arias intensity (Rezaeian and Der Kiureghian 2012), is the highest. The major principal axis is assumed horizontal and pointing towards the direction of the earthquake source (Penzien and Watabe 1975). However, this hypothesis appears not to be always verified, especially in a near field regime (as further recent investigations by Rezaeian and Der Kiureghian 2012 proved). Assuming quasi-vertical ground motion and the vertical component as the less intense, the second horizontal principal component is denoted as the *intermediate principal component* (int) (Rezaeian and Der Kiureghian 2012; Penzien and Watabe 1975). Figure 9 shows the mentioned cross-correlation coefficient varying with the in-plane rotation angle $\rho_{XY}(\theta_{XY})$ for two selected records at SG1 (for KSH site) and at G51 (for KK5 site). Penzien and Watabe (1975) examined the correlation coefficient ρ_{XY} for a number of recorded ground motions, varying the angle θ_{XY} by which the in-plane components are rotated. They did not observe a significant time-dependence so that ρ_{XY} was computed for the entire length of the record. For each signal, the *correction angle* θ_C refers to the in-plane rotation angle at which ρ_{XY} vanishes, thus defining major and intermediate axes at that depth. Such an angle (the solid black line in Fig. 9) was compared to θ_{BB} and to θ_{NP}, where θ_{BB} corresponds to the correction angle computed at the deepest sensor in the array (SG4 and G55 respectively), whereas θ_{NP} is measured between seismometers and

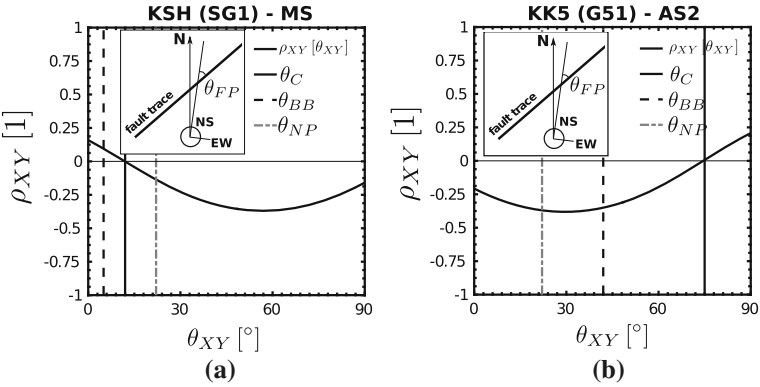

Fig. 9 Cross-correlation coefficient ρ_{XY} varying with rotation angles θ_{XY} angle at SG1/G51. θ_C makes the $\rho_{XY} = 0$ at the considered depth. θ_{BB} (black dashed line) represents the angle corresponding to $\rho_{XY} = 0$ for accelerometers **a** SG4 and **b** G55 respectively. θ_{NP} (grey dotted line) is the angle between the strike directions of the fault and the seismometers' reference system

fault plane strike directions (see the miniature in Fig. 9b). For the main shock (Fig. 9a) θ_C values calculated for array KSH are coherent with the those estimated by Pavlenko and Irikura (2012). They corrected the orientations of the sensors based on the recorded low-frequency (0.01–0.2 Hz) trajectories within a 3 s-wide window located just after the first wave arrival time. They obtained correction angles θ_C of 6°, 8°, 4° for sensors SG2, SG3 and SG4 respectively. θ_C and θ_{BB} are close to θ_{NP} when considering the main shock, confirming somehow a dominant direction of the motion (i.e. towards the fault asperities). In this sense, maj-int directions align to the FN/FP ones.

This is not true for the aftershocks sequence, e.g. for aftershock 2 (see Fig. 9b), where the three mentioned angles differ one from each other.

However, the fact that $\theta_C \neq \theta_{BB}$ in both cases may be due to the local geological conditions that deviate the principal axes of motions from down-hole towards the surface.

3 Identification of non-linear site-effects

The aim of this section is the identification of those features of recorded ground motions, both during the main shock and the aftershocks, that may support the evidence of non-linear soil response. A first hint of non-linearity taking place is given by plots in Fig. 10, where a Site Amplification Function (SAF) is introduced as the ratio of PGA at ground surface with respect to the corresponding PGA at depth (PGA_R). Site Amplification Factors were computed at KSH and KK5 by considering two couples of seismometers each: (1) SG1–SG2 at G.L. − 2.4 m and G.L. − 50.8 m and SG2–SG4 at G.L. − 50.8 m and G.L. − 250 m respectively at KSH; (2) G51–G52 at G.L. − 2.7 m and G.L. − 36 m and G52–G55 at G.L. − 36 m and G.L. − 312 m respectively for KK5. In the case of linear response, the trend of SAF would be constant, independent of PGA_R, supposed not to be affected by non-linearity. As a matter of fact, on one side the KK5 array shows this trend, having recorded only the aftershocks (Fig. 10c, d), while, on the other side, KSH shows a clear tendency to a decreased SAF for increasing PGA_R beyond about 0.1 g (Fig. 10a, b), which is often considered as the threshold for significant non-linear response in soft soils (Kramer 1996).

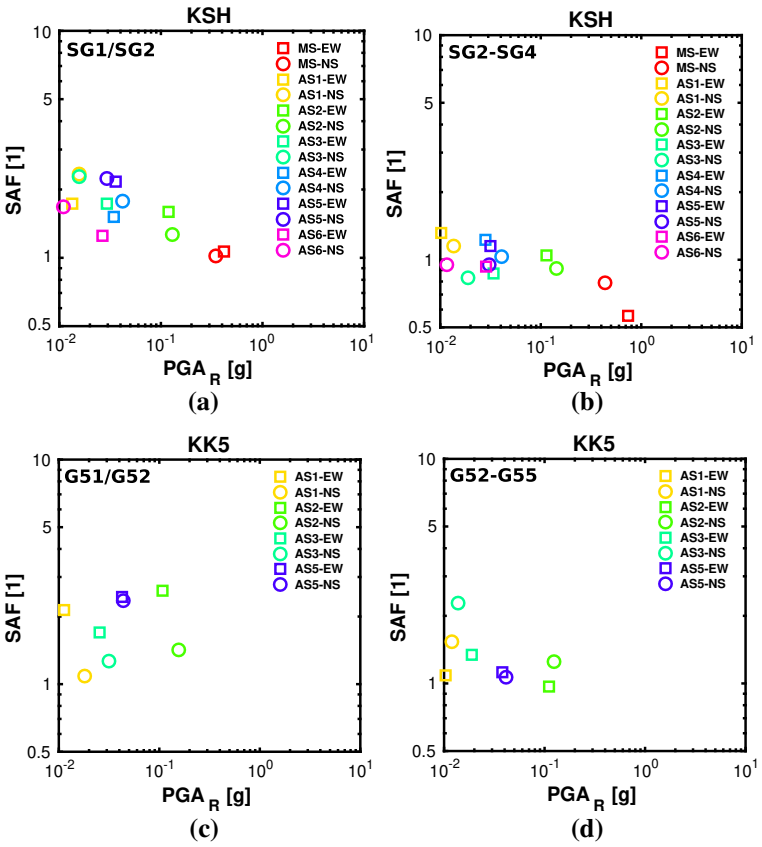

Fig. 10 Site Amplification Factors (SAF) computed on PGA at KSH (**a**, **b**) and KK5 (**c**, **d**) array, with respect to the PGA recorded at bedrock. **a** SAF considering SG1/SG2 ratio (KSH), **b** SAF considering SG2/SG4 ratio, **c** SAF considering G51/G52 ratio (KK5), **d** SAF considering G52/G55 ratio (KK5)

The latter tendency is observed not only when considering the shallowest instrument (SG1), but also when considering SG2, placed at G.L. − 50.8 m, meaning that non-linear effects may have occurred below this depth. The presented results agree with the results presented by Pavlenko and Irikura (2012). The authors concluded that the motion at the Service Hall was de-amplified during its propagation to the surface from the depth of 250 m because of the non-linearity of the soil response. At the same time, at Unit 5 the ground motion was amplified on the surface if compared to the motion at 200–300 m, indicating that the seismic waves resonant amplification prevailed.

3.1 Validation of shear-wave velocity profile

The entity of recorded seismic site-effects strongly depends on the initial, small strain shear wave velocity values and on the spatial distribution of geological layers. To this end, in situ measurements represent a good estimation of the initial profiles. Down-hole methods (such as PS-logging) are generally considered the most accurate and direct (invasive) measurement of the shear wave velocity, but their estimation may be biased by the

soil disturbance (as observed by Thompson et al. 2009). Moreover, the upward propagating wave motion alters the mechanical properties of shallow sediments, reducing their stiffness and increasing their damping capacity. Those alterations may be irreversible sometimes. For these reasons, the first investigation consisted into estimating V_S variation along the strong motion duration. A *seismic interferometry* technique was applied to the available records (Curtis et al. 2006). Briefly, this technique consists of computing the wave travel-times between two adjacent sensors, estimated as the lag-time at which the seismic interferogram attains its peak. In 1D Earth-like models, only a single wave source is considered to construct those seismic interferograms (cross-correlation between two recorded signals in function of lag-time) between any source-receiver pair, including sources or receivers placed on the free surface (Curtis et al. 2006). A sliding time window of 4–6 s (with 50% of overlap) was selected. Base line correction and Hanning tapering (5%) were performed on the windowed signals.

Figure 11 presents V_S values varying with time, at Service Hall and Unit 5 respectively. At shallow depths (i.e. within the first 50 m under the surface, which is the distance from instruments SG1 and SG2) a consistent V_S reduction may be observed after the main shock arrival (array KSH). Values are substantially lower than the minimum value at SG1 ($\cong$ 310 m/s), especially along the NS direction (probably due to a non-linear anisotropic soil behaviour and to the ground motion incoherence due to near-field conditions). Shear wave velocity does not seem to retrieve its original value within the first meters under the surface, at least for the first 150 s of MS (Fig. 11a). On the other hand, the most intense aftershock did not cause a significant degradation of shear modulus, as we can notice in Fig. 11b. A reduction at *intermediate* depths can be observed too at KSH (in the strata between SG2 and SG3's depths, Fig. 11c), whereas no reduction occurred at KK5 (Fig. 11d). Reduction could be neglected for stiffer sediments. In Fig. 12, estimated V_S profiles are compared to PS-logging estimations provided by the TEPCO.

Results from the aftershocks overestimate PS-log V_S profile: this is probably due to scarce resolution of the method for ground motions of weak intensity. Aftershock 2 seems not to degrade significantly the soil mechanical properties. However, borehole interferometry analysis is limited by the coarse distribution of recording devices along depth. Suspension logging measurements performed at KSH by Yee et al. (2011) also revealed V_S values between 130 and 240 m/s within the first 16 m depth, followed by values ranging between 240 and 390 m/s till 70 m depth finally the bedrock materials have velocities increasing from 330–450 (between 70 and 83 m) to 400–600 m/s (for depths greater than 83 m). Seismic interferometry revealed a stiffness reduction within the shallowest soil layers for main shock at KSH, while computed and measured shear wave values are similar at KK5. Tokimatsu and Arai (2008) back-calculated the shear wave velocity values by coupling genetic algorithms with the equivalent linear method. Their findings showed shear wave velocities at depths smaller than about 70 m significantly smaller than the PS-logging measures (even for small aftershocks). In contrast, those at deeper depths for the three events are almost identical. Those results make the PS-logging profiles questionable. The estimated V_S profiles may be used as simplified geology configuration for numerical models. The described behavior was remarked by several authors. For instance, Pavlenko and Irikura (2012) estimated a 30–35% reduction of the shear modulus within the first 42 m down-hole, during the main shock. Mogi et al. (2010) estimated temporal changes of S-wave velocity by using Normalized Input–Output Minimization (NIOM) method based on the vertical array records observed during the main shock and the events before and after it and found that the S-wave velocity in the layers (0–50 m) and (50–100 m) decreased significantly during the principal motion of the main shock (indicating non linear

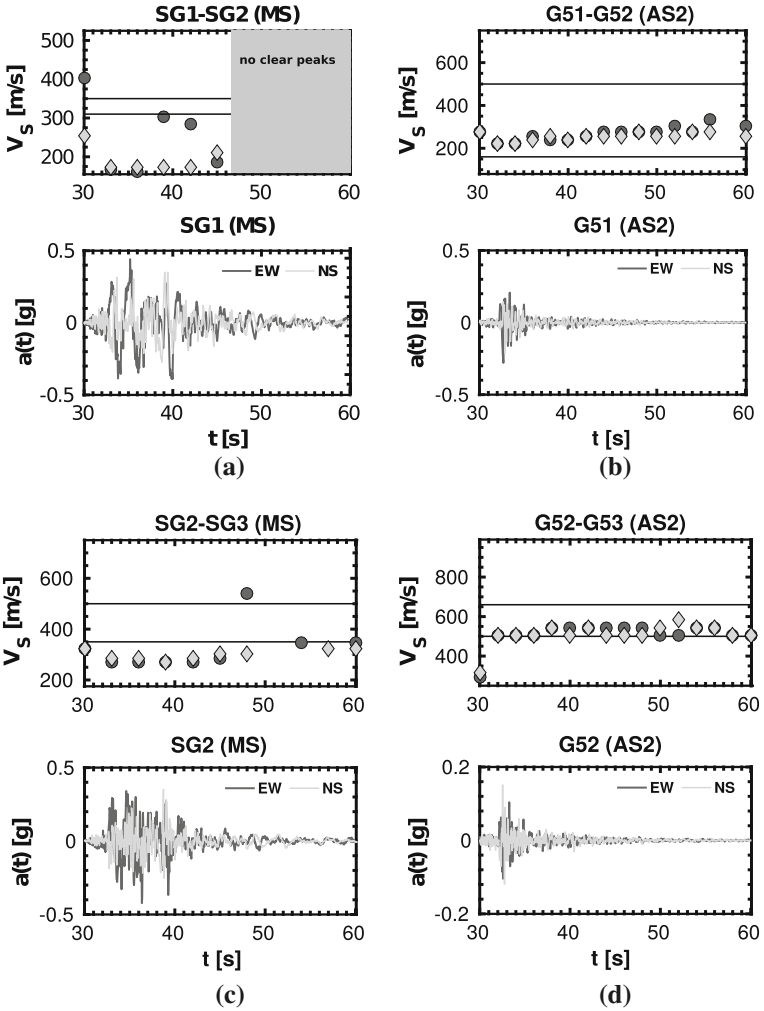

Fig. 11 V_S values estimation by borehole interferometry (along the EW-NS directions, dark grey circles and light grey diamonds, respectively); solid black lines indicate average V_S values (from PS-log) at the two devices' locations. The EW-NS time-histories are also shown, for **a** main shock at KSH (seismometers SG1-SG2), **b** aftershock 2 at KK5 (seismometers G51-G52), **c** main shock at KSH (seismometers SG2-SG3), **d** aftershock 2 at KK5 (seismometers G52-G53)

behaviour), whereas nearly linear behaviour was observed in the bedrock layer (below 100 m).

4 1D numerical simulations of soil response

As stated in Sect. 3, non-linear de-amplification occurred in the high-frequency part of ground motion (especially in terms of PGA) during the 2007 Chuetsu-Oki main shock strong motion earthquake, whereas aftershock sequence caused negligible degradation of

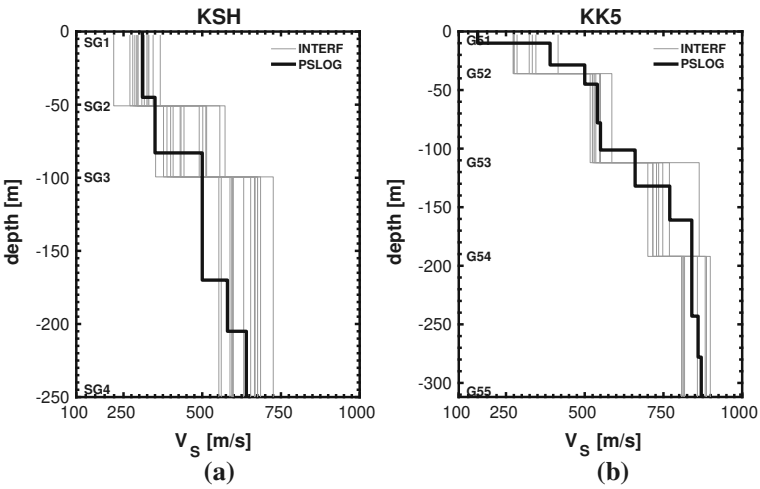

Fig. 12 V_S profile obtained by averaging EW–NS results from borehole interferometry analysis on the two arrays KSH (instruments SG1 to SG4 at depths G.L. − 2.4, − 50.8, − 99.4 and − 250 m respectively) and KK5 (instruments G51 to G55 at depths G.L. − 2.7, − 36, − 112, − 192 and − 312 m respectively). Computed profiles are compared with the PS-logging one (black line) provided by TEPCO (2008)

soil stiffness. To complete the site characterization, 1D numerical simulations were performed in two stages: (1) verification of the stratified geological profile and site seismic response at small strains (i.e. analyses on the aftershocks sequence); (2) validation of available $G/G_{max} - \gamma - D$ curves by standard equivalent linear approach (EQL). The first stage of the analysis aims to compare the discontinuous shear modulus profiles released by TEPCO (PS-logging measures plotted in Fig. 6) with modified ones, in terms of empirical borehole spectral ratio (BHSR). In both cases the wave equation is solved in the frequency domain, but in the EQL formulation the shear modulus and damping ratio are iteratively adjusted as a function of an effective measure of shear strain (Kramer 1996).

The two soil column models defined for KSH and KK5 respectively, reach the depth at which sensors SG3 and G52 were installed, i.e.G.L. − 99.4 m for KSH and G.L. − 36 m for KK5 (see Figs. 6, 13).

For this purpose, two real accelerograms are available to compare the result of numerical simulation. Furthermore, EQL formulation is generally suitable to characterize the seismic response at shallow depths, where the hypothesis of quasi-vertical propagation of the seismic input holds approximately (see Sect. 2). The use of EQL 1D approach probably is not the most appropriate for these profiles where the *seismic bedrock* with $V_S > 800$ m/s is quite deep (> 100–200–300 m) and the surface soil quite *soft*. However, most of PGA values observed at surface during the main shock values fall outside the spectral zone delineated by Kaklamanos et al. (2013) based upon the statistical analysis of 100 Kik-Net sites, where the EQL becomes inconsistent and a fully non-linear site analysis is rather suggested (Fig. 14). Just two of the analyzed records effectively fall into the mentioned area, granting a priori the possibility of using EQL, to quantify the main aspects of such complicated non-linear site effects by employing traditional engineering tools.

Real base-line corrected recordings were introduced, under the assumption of *within input motions* (Kwok et al. 2007). To overcome the limitation of 1D numerical analyses to be dependent on the input motions and therefore to tackle the dependence of the observed

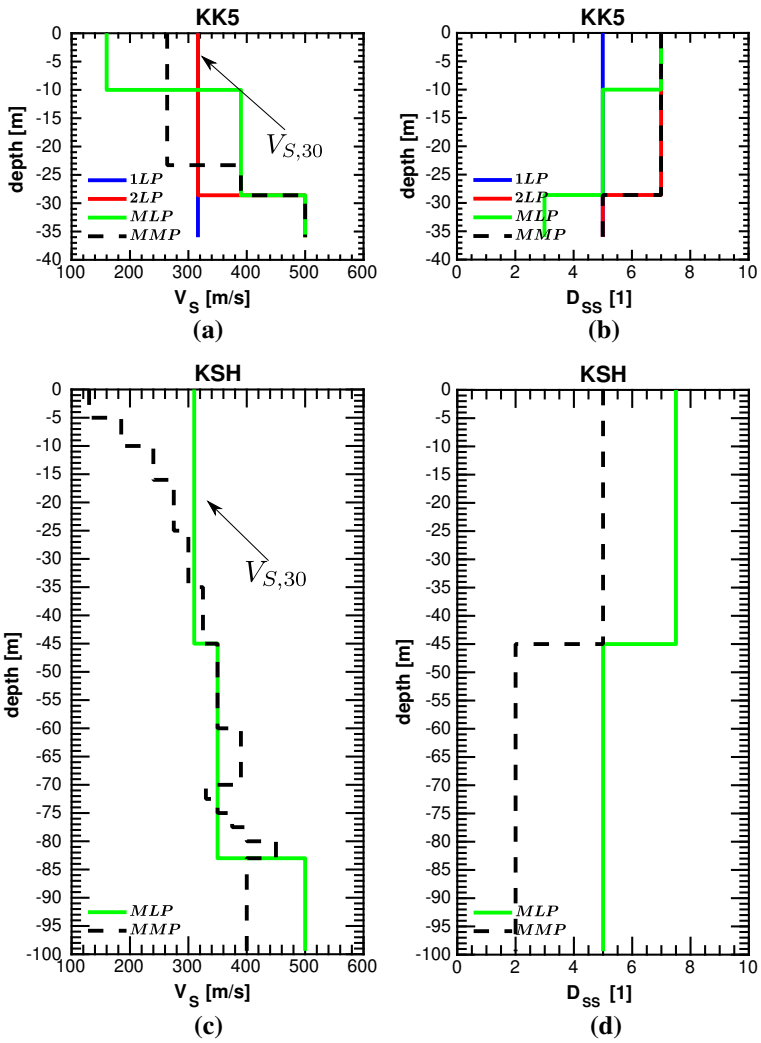

Fig. 13 Simplified V_S and small-strain damping (D_{SS}) profiles used in the analysis herein. **a–c** V_S profiles for KK5 and KSH soil column models, **b–d** small strain damping D_{SS} for KK5 and KSH soil column models. 1LP and 2LP are a mono- and bi-layer profiles respectively. MLP profiles corresponds to the PS-logging measurements provided by TEPCO (2008). MMP are the adjusted profiles adopted in the further sections for equivalent linear analysis

site response on the direction considered (see Sect. 2), results were post-processed by applying common averaging techniques used in seismology. For instance, theoretical borehole spectral ratios are compared to the geometric mean [called EMP-GM, defined in Eq. (3)] of the ensemble of spectral ratios computed for N_θ different in-plane rotations of the two horizontal components (by an angle $\theta_n \in [0^\circ; 180^\circ]$), namely

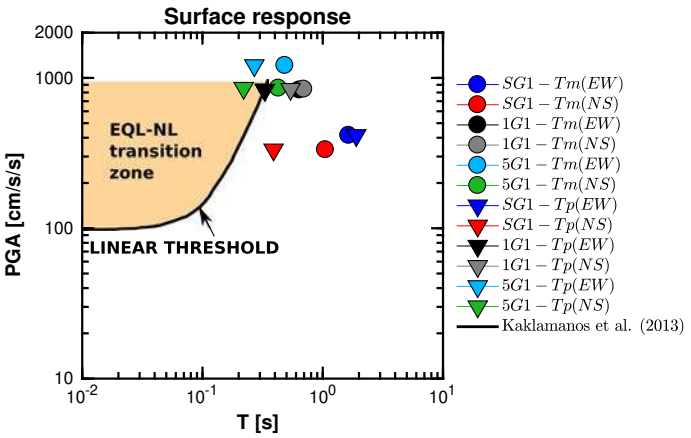

Fig. 14 Observed PGA at ground surface (SG1, 1G1 and 5G1) at mean period Tm (circles) and predominant period Tp (triangles) (Rathje et al. 1998). The linear threshold defines the zone where the Equivalent Linear Method has to be dropped in favor of fully non-linear analysis (according to Kaklamanos et al. 2013). Kaklamanos et al. (2013) did not provide indications for PGA > 981 cm/s^2

$$EMP - GM(f) = \prod_{n=1}^{N_\theta} \sqrt[n]{\left(\frac{O_X(f,\theta_n)}{I_X(f,\theta_n)}\right)\left(\frac{O_Y(f,\theta_n)}{I_Y(f,\theta_n)}\right)} \tag{3}$$

where $O_X(f,\theta_n)$, $O_Y(f,\theta_n)$ represent the Fourier ordinate of recordings at shallowest depth at frequency f, considering two horizontal orthogonal directions X and Y respectively, obtained by a rotation of angle θ_n of the as-recorded EW-NS components. $I_X(f,\theta_n)$, $I_Y(f,\theta_n)$ refer to deepest recording station.

Similarly, the geometric mean of the two horizontal 5% damped elastic spectral ordinates in acceleration at period $T(Sa_{GM}(\theta))$ is obtained. In equivalent linear analyses, numerical results depend on the different rotation angles θ at which the input motion were injected at the soil-column base. Therefore, the response spectra geometric mean between each couple of rotated components X–Y obtained numerically (one couple for each θ) is first computed. Then, geometric mean (called GM-EQL) and 16th–84th percentiles of $Sa_{GM}(\theta)$ are compared to the *Sa* obtained from original records (EW/NS components) at the shallowest stations in the arrays (SG1 and G51 for KSH and KK5 respectively).

4.1 Seismic response at KK5

4.1.1 Seismic response in small strain regime

In the surroundings of Unit 5, in situ measurements found a shallow subsurface layer of over-consolidated clay overlying the engineering bedrock. Gatti et al. (2015) observed some discrepancies when using the PS-logging measurements (provided by TEPCO) at shallow depths, at Unit 5 array. They compared empirical transfer functions with the theoretical ones, obtained with the original V_S profile, provided by TEPCO, and called *Multi-Layer Profile* (MLP) with two simplified profile, *Two-Layers Profile* (2LP) obtained by *smoothing* the two shallow layers of MLP (i.e. replacing them with $V_{S,30}$ value) and *One-Layer Profile* (1LP), with $V_{S,30}$ uniform value. Those findings have been extended hereafter, by introducing a further modified profile (MMP) (black solid lines in Fig. 13a,

b). In Fig. 15, theoretical transfer functions (called *borehole spectral ratios*, BHSR) are compared to the empirical geometric mean (orange thick line labelled as EMP-GM) and to the 16th–84th percentiles.

Results presented in Fig. 15 show the achieved effect due to the adjustment of the provided profile. Profile MMP seems to be the best compromise, at least for the weakest aftershocks such as AS1 and AS3 (Fig. 15a–c): the related theoretical transfer function matches satisfactorily the first two peaks of the EMP-GM transfer function. This result supports the importance of the impedance contrast between the deepest stiff layer ($V_S = 500$ m/s) and the shallowest ones. However, slight discrepancies between simulated and recorded soil response are still pronounced as provided in Fig. 15b, where it can be seen that the simulated spectral ratios fit rather well the recorded ones in two cases (AS1 and AS3), while in the other ones (AS2 and AS5) the observed spectral ratio shows peaks at a lower frequency than the simulated ones. On one side, it may be argued that the shift of the observed peak towards lower frequencies may be due to the onset of significant non-linear effects (as a matter of fact, AS2 is the most intense aftershock). On the other side, other factors may affect the position and amplitude of the peaks of seismic response for

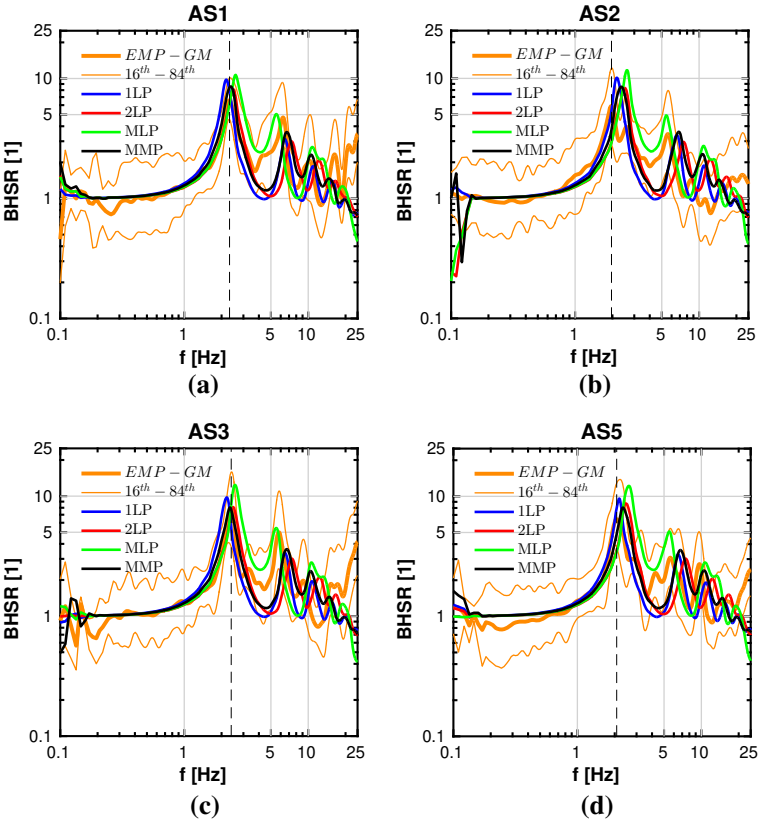

Fig. 15 Theoretical transfer function for borehole KK5, compared to the Empirical ones along the generic X–Y directions for **a** aftershock 1, **b** aftershock 2, **c** aftershock 3 and **d** aftershock 5. EMP-GM represents the geometric mean transfer function on different in-plane rotation angles. 16th–84th percentiles of Empirical borehole spectral ratios are plotted as thin orange lines. 1LP, 2LP, MLP and MMP refer to one-layer, two-layer, multi-layer and modified-multi-layer profiles respectively

weak motions, such as the frequency dependence of damping (e.g. Miura et al. 2000), which is commonly considered constant in the 1D equivalent linear simulations. In the present case, a satisfactory match with observed spectral ratios was found using hysteretic damping ratio of about 7% (see Fig. 13b), which is substantially larger than expected at small strain. This implies the underestimation of higher modes.

4.1.2 Equivalent linear analysis

For borehole KK5 two aftershocks are considered to reproduce non-linear site effects (i.e. AS2 and AS5), since they exhibited period lengthening (as mentioned in previous subsection), with respect to the linear visco-elastic approach. Unfortunately, records of NCO main shock went lost.

A few information on the dynamic properties of the soil deposits at this site were released by the TEPCO, namely: (1) a set of normalized secant shear modulus reduction and damping curves for the shallower clayey deposits (curve *Clay Ref.* in Fig. 16) and (2) a set of curves referring to the so called *engineering bedrock* (curve *Rock*).

As observed by many authors (e.g. Vardanega and Bolton 2013; Darendeli 2001) the cyclic behaviour of over-consolidated clays is affected by the confining pressure to some extent. TEPCO did not specify the reference confinement pressure for which the non-linear model curves were issued, so a conventional value of 100 kPa was assumed and a stress-wise correction was applied consequently. The latter was inspired by Pecker (2011), who proposed to relate the variation of the dynamic non-linear properties to the effective overburden vertical stress σ'_{V0}. For instance, they presented two new sets of curves, referring respectively to σ'_{V0} 75–125 kPa and portrayed in Fig. 16, under the tag *Clay 75 kPa* and *Clay 125 kPa*. Figure 16 compares the mentioned experimental curves with the set of curves selected in the equivalent linear analysis, performed on MMP V_S model (see Fig. 13). The stress-wise correction unwraps into two steps: (1) interpolating the

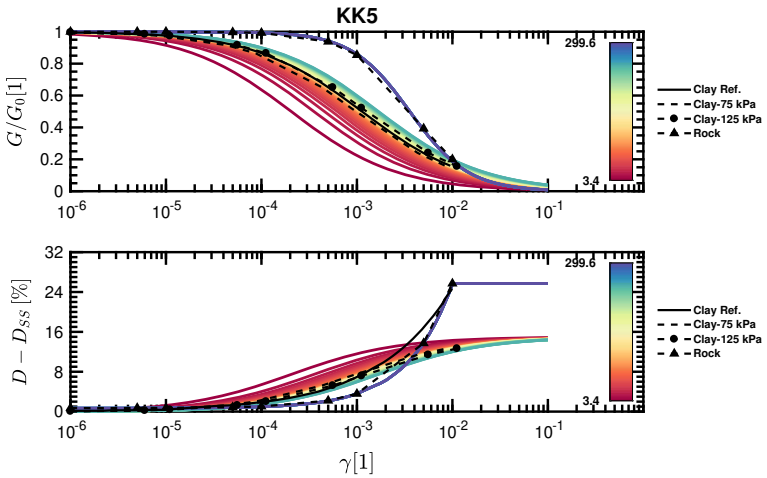

Fig. 16 $\frac{G}{G_{max}} - \gamma - D$ curves for KK5 site. Experimental data from laboratory tests (*Clay Ref.* and *Rock*, courtesy of TEPCO) are compared to curves used in equivalent linear analysis (MMP V_S profile). Damping values are discounted from the small strain critical damping D_{SS} relative to each layer and taken from MMP model. The color bar refers to the vertical stress state estimated along the borehole depth

experimental points of the reference curve by employing the backbone curve model proposed by Nakagawa and Soga (1995); (2) correcting the calibrated parameters by a factor $\sqrt{(\sigma'_{V0}/p_{atm})}$, according to Pecker (2011) (with σ'_{V0} being evaluated at the middle of each soil layer and p_{atm} being the atmospheric pressure). In details, the shear modulus degradation curve is casted into the following bi-parametric equation:

$$\frac{G}{G_{max}}\left(\sigma'_{V0}\right) = \frac{1}{1+\alpha\left(\gamma\sqrt{\frac{p_{atm}}{\sigma'_{V0}}}\right)^{\beta}} \tag{4}$$

Stress dependency was also assumed for the non-linear evolution of critical damping ratio as follows:

$$D\left(\sigma'_{V0}\right) = D_{SS} + D_{LS}\left(1 - \frac{G}{G_{max}}\left(\sigma'_{V0}\right)\right) \tag{5}$$

where D_{SS} and D_{LS} indicate small- and large-strain damping ratios respectively (set respectively to 5 and 15%). The corrected hysteretic damping at large strain was forced to saturate, in agreement with the adjustments proposed by Darendeli (2001). α and β were obtained by logarithmic interpolation of the reference curve released by TEPCO (*Clay ref.*). The modified $\frac{G}{G_{max}} - \gamma - D$ curves were associated to the first 25 m of the MLP model (over-consolidated clays). The deepest layer (defined by V_S of 500 m/s) was associated to the *Rock* degradation curve, interpolated over the experimental data.

Numerical prediction and recorded response are compared in Fig. 17 in terms of acceleration time-histories and in Fig. 18 in terms of elastic response spectra in acceleration *Sa*.

An overall good agreement is observed between simulated time-histories and the recorded ones for AS2 and AS5. In terms of spectral ordinates however, EQL analysis provides a slightly damped *Sa* spectrum, compared to the recorded one (Fig. 18b). This

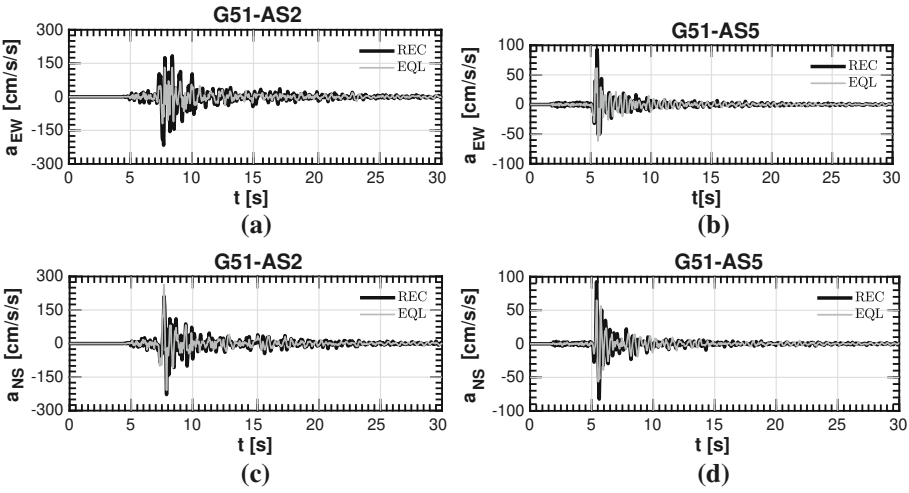

Fig. 17 Comparisons between acceleration time-histories recorded and simulated (by equivalent linear analyses and angle $\theta = 0^{\circ}$) time-histories for AS2 (**a–c**) and AS5 (**b–d**) at KK5 site

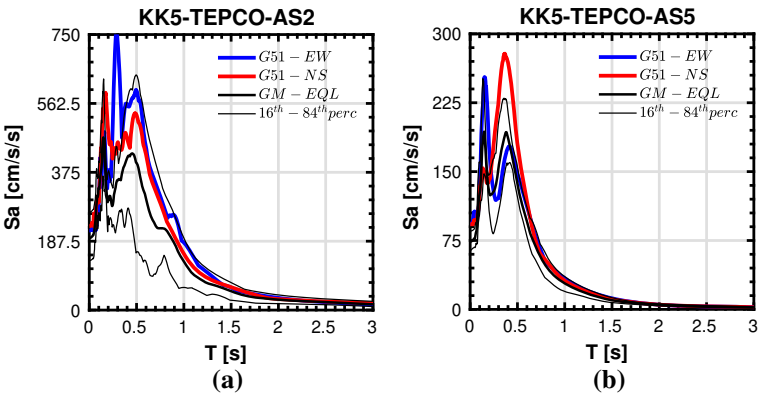

Fig. 18 Elastic response spectrum in acceleration *Sa* (conventional damping 5%) referring to AS2 (**a**) and AS5 (**b**) at KK5 site. Thick solid black lines (GM-EQL) refers to the results from equivalent linear analyses, being the geometric mean of all the $Sa(\theta)$. Finer solid black lines represent the 16th–84th percentiles of $Sa(\theta)$ distribution. Blue and red lines refer to the recorded EW–NS response accelerations

might be due to the recovered stiffness of the clayey deposits at shallow depths. The chosen stress correction may play a major role as well. For AS2, some discrepancies at shorter periods can be noticed, e.g. the peak at approximately 0.3 s along the EW direction in Fig. 18a. As a matter of fact, EQL simulations well captured the dependency of the spectral ordinates on the rotation angle of the input motion only for periods longer than 0.4 s.

4.2 Seismic response at KSH

4.2.1 Seismic response in small strain regime

The site response at the Service Hall was simulated according to the same approach as for KK5 site. The TEPCO V_S profile (MLP, portrayed by the green lines in Fig. 13c, d), based on an earlier suspension logging campaign, was compared to the estimation made by Yee et al. (2011) (MMP, portrayed by the dashed black lines in Fig. 13c, d), obtained by integrating new PS-logging measurement with Standard Penetration Tests performed by the Tokyo Soil Research in 2009 at the Service Hall site. The soil deposits are mainly composed of unsaturated and poorly graded sands till 70 m. Below this depth, for both geological models, the unit weights at different depths were retrieved from in situ and laboratory results performed by Yee et al. (2011). The MLP layered geological model is poorly refined at shallow depths, compared to the MMP model, which is also featured by a velocity inversion below 70 m. As expected from the interferometry results (Sect. 3.1 and Fig. 12) the MMP model looks more adequate in reproducing the empirical borehole transfer function (Fig. 19), both in terms of the main natural frequency peak for weaker (AS3) and more intense aftershocks (AS2).

Higher models are better reproduced by the MMP layering configuration, although de-amplification and shift towards the lower frequencies is observed for AS2. For MLP, the critical damping values provide a decrease of the frequency peaks much larger than observed. However, the D_{SS} values employed represent the *best* compromise for MLP profile to match the first mode. As a matter of fact, Yee et al. (2011) highlighted that the

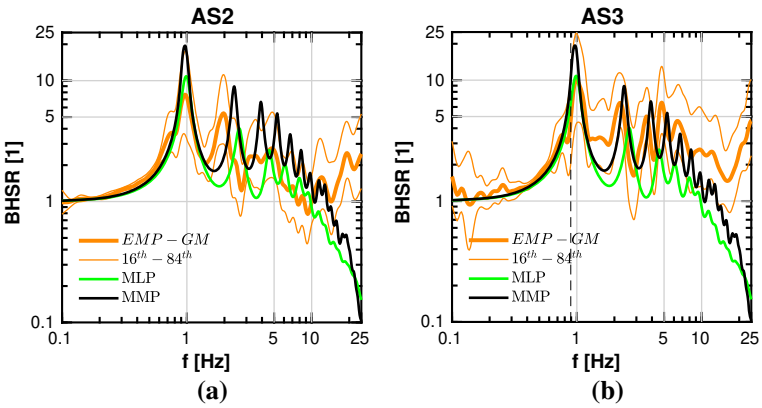

Fig. 19 Theoretical transfer function for borehole KSH, compared to the Empirical ones along the generic X–Y directions for **a** aftershock 2 and **b** aftershock 3. EMP-GM represents the geometric mean transfer function on different in-plane rotation angles $\theta \in [0^{\circ}; 180^{\circ}]$. 16th–84th percentiles of Empirical borehole spectral ratios are plotted as thin orange lines. MLP and MMP refer respectively to multi-layer and modified-multi-layer profiles respectively

as-provided model-data (from the previous studies performed by TEPCO on this site) showed some over-prediction of motions at G.L. − 2.4 m (device SG1), which they referred to an underestimation of damping ratios (ranging between 1 and 4%), which they also observed in their resonant column tests. Thus, they slightly increased D_{SS} to 2–5%. However, results does not clearly support either a preferential choice on MLP or MLP, probably due to the greater depth reached by the soil column model (i.e.G.L. − 99.4 m) where recording device SG3 is installed and to some residual modification of the soil properties, due to the strong main shock that struck the site.

4.2.2 Non-linear site response at KSH

The borehole array KSH, installed at the KK-NPP Service Hall, recorded the NCO main shock. Nonetheless, according to Yee et al. (2011), prior to the 2011 Tohoku Japan earthquake, the KSH array recorded the strongest motions for a vertical array in soil, without exhibiting liquefaction. Therefore, this location is suitable to study the non-linear site response in the surroundings, via 1D soil column analyses. Main shock (MS) and aftershock 2 (AS2) are considered herein.

TEPCO released a degradation curve for sand layer (*Sand ref.* in Fig. 20). Those values were assumed to refer to an in situ confining pressure state of 100 kPa. The stress correction described in Sect. 4.1 was judged incompatible with the experimental results obtained by Yee et al. (2011) (curves tagged as Yee et al. in Fig. 20).

A more accurate description of the effect of the overburden pressure was proposed by Yee et al. (2011), so to fit the laboratory results. The authors adopted a classical hyperbolic model (Hartzell et al. 2004), in the form of:

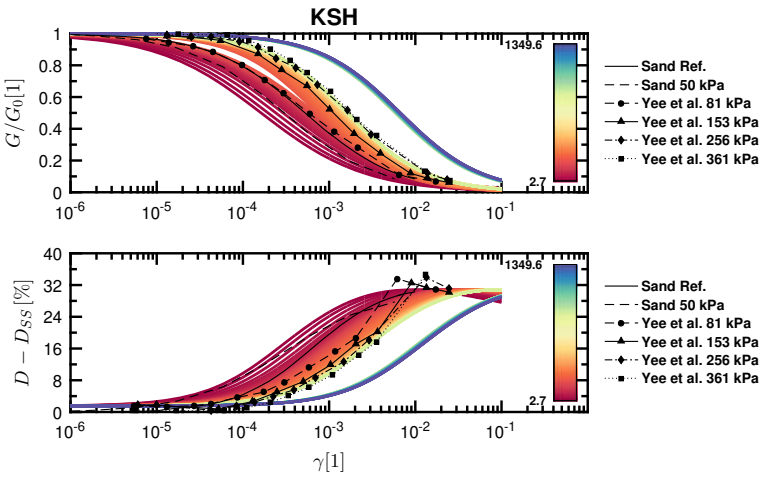

Fig. 20 $\frac{G}{G_{max}} - \gamma - D$ curves for KSH site. Experimental data from laboratory tests conducted by the Tokyo Soil Research (Yee et al. 2011) and by TEPCO are compared to curves used in equivalent linear analysis (MLP profile), obtained by applying the overburden stress correction proposed by Yee et al. (2011)

$$\frac{G}{G_{max}}\left(p_0^{'}\right) = \frac{1}{1 + \left(\frac{\gamma}{\gamma_r\left(p_0^{'}\right)}\right)^{\beta\left(p_0^{'}\right)}} \tag{6}$$

where γ_r represents the pseudo-reference shear strain and $p_0^{'}$ the mean effective confining pressure at depth. Based on the previous parametric studies performed by Menq (2003) on the dynamic properties of cohesion-less granular soils, they adjusted the provided empirical relations by proposing the following stress dependencies for γ_r and β:

$$\gamma_r\left(p_0^{'}\right) = \gamma_{r,1}\left(\frac{p_0^{'}}{p_{atm}}\right)^n \tag{7}$$

$$\beta\left(p_0^{'}\right) = \beta_1 + \beta_2 log\left(\frac{p_0^{'}}{p_{atm}}\right) \tag{8}$$

$\gamma_{r,1}$, n, β_1 and β_2 are regression coefficients, which have been tuned upon the experimental results for the unsaturated sandy deposit above 70 m (approximately corresponding to a confining pressure $p_0^{'} = 6.75$ atm), whereas at higher depths they assume the empirical values obtained for clays by Darendeli (2001). However, the inherent uncertainty on those regression coefficients reported by Yee et al. (2011) was solved by a trial and error adjustment, at each depth. Figure 21a, b portray the comparison between the adopted values of γ_r and β with varying confining pressure (referred as to $Y - mod.$) along with the models proposed by Yee et al. (2011) (average value $Y - \mu$ and confidence limits $Y - \mu \pm \sigma$).

Figure 21 highlights the two main major adjustments adopted herein: (1) γ_r deviates from the Yee et al. (2011) exponential model at small confining pressures (i.e. $p_0^{'} < 2$ atm) so to better capture the experimentally measured pseudo-reference strain; (2) β values generally range across the lowest curve ($Y - \mu - \sigma$).

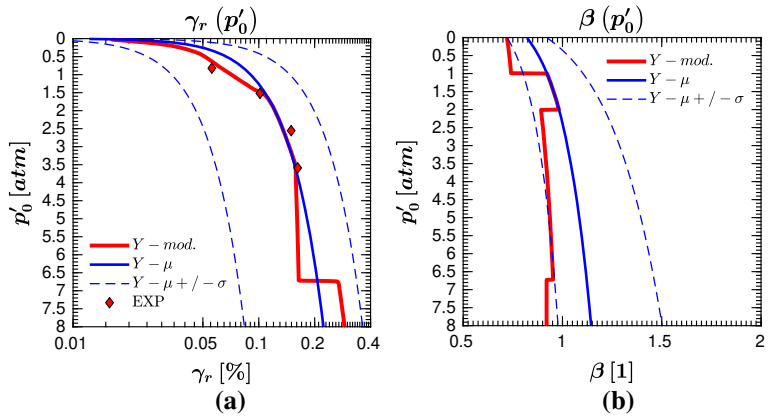

Fig. 21 Values of γ_r (**a**) and β (**b**) with varying confining pressure p'_0. Red lines referred as to $Y - mod.$ indicate the stress correction employed in this study. Blue lines refer to the average ($Y - \mu$) values and confidence limits ($Y - \mu \pm \sigma$) of the regression coefficients according to Yee et al. (2011). The red symbols indicate the laboratory results reported by Yee et al. (2011)

Thanks to those quite simple expedients, the simulated time-histories (see Fig. 22) are rather well reproduced, despite the higher frequency content *polluting* the simulations and mainly due to the limitations of the equivalent linear method with intrinsic hysteretic assumption of a frequency-constant damping (Miura et al. 2000, among others).

In Fig. 23 simulated site response for MS is strongly dependent on the direction along which the motion is projected.

The MS recorded response spectra are well replicated for natural periods greater than 2.0 s, EQL results show high variability depending on the input motion angle considered at shorter periods. On the other hand, for AS2 the simulated response ranges within a narrow

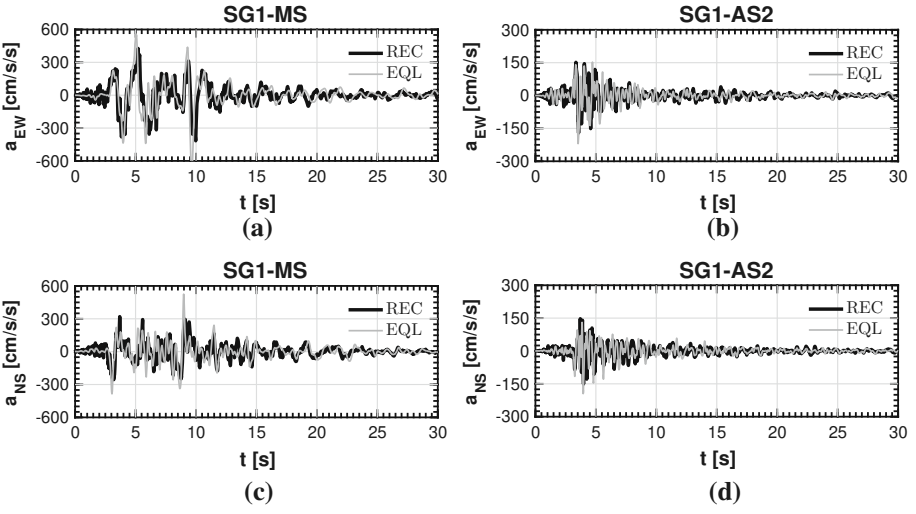

Fig. 22 Comparisons between acceleration time-histories recorded and simulated (by equivalent linear analyses) for MS (**a**–**c**) and AS2 (**b**–**d**) at KSH site

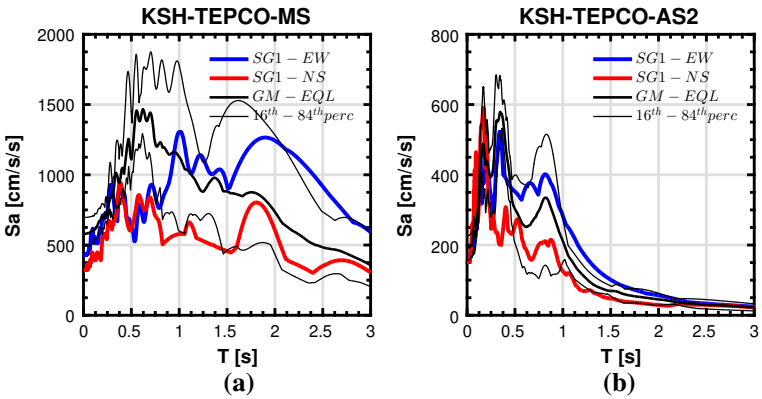

Fig. 23 Elastic response spectrum in acceleration *Sa* (conventional damping 5%) referring to MS (**a**) and AS2 (**b**) at KSH site. Thick solid black lines (GM-EQL) refers to the results from equivalent linear analyses, being the geometric mean of all the $Sa(\theta)$. Fine solid black lines represent the 16th–84th percentiles of $Sa(\theta)$ distribution. Blue and red lines refer to the as-recorded EW-NS response accelerations

confidence band across GM-EQL (Fig. 23). Those effects are related to the proximity of the seismic source, as the relatively high spectral response at long period confirms and since the motion intensity and direction change drastically the response. Moreover, those discrepancies highlight the shortcomings of EQL analysis when large strains occur. For the MS, some strain localization occurred, ranging beyond the usable limit of the backbone curves (obtained by Resonant Column tests), mostly due to the abrupt drop V_S close to the surface (Yee et al. 2011).

5 Conclusions

The *Niigata-Ken Chūetsu-Oki* earthquake affected the Kashiwazaki-Kariwa Nuclear Power Plant, causing limited damage to the nuclear installments. Non-linear site effects were observed (e.g. large settlements, seismic motion de-amplification). The case study was very interesting either from a seismological point of view, either from an engineering one. The latter was adopted in this study, tackling some crucial features of the global seismic response of KK-NPP.

First of all, since the design seismic capacity has been exceeded during the main shock, a correlation between the recorded peak values (i.e. PGAs) and the dominant harmonic periods of the ground motion was established, proving the potential damage occurrence at some locations within the site. In the following, the impulsive response of the incoming wave field was assessed. *Hanging wall* and *directivity* effects were judged as responsible of such a response, due to the small source-to-site distance. These characteristics of the seismic scenario prevent the recognition of preferential direction of motion, i.e. making the site response strongly dependent on the considered horizontal direction at each location.

The consistent number of recordings available was exploited to check whether non-linearity took place. Wave motion de-amplifies towards the surface, as expected during the main shock. Moreover, non-linear stiffness degradation was observed at shallow depths, thanks to seismic interferometry applied to borehole arrays of seismometers. Thus, PS-logging measurements referring to this specific site are found to be poorly reliable for the

seismic response analysis at the reactor building. V_S values measured in situ may overestimate the real soil stiffness during transient analyses. This is confirmed by the equivalent linear calculations presented in Sect. 4: predicted transfer functions provide a reasonable match to the shape and resonant frequencies of the observed ones, although the data is clearly too limited to establish statistically significant empirical trends for small-strain site response. Original mechanical properties may have not been recovered during the aftershock cluster, preventing the use of weak motions as input for calibration of non-linear soil models. On the other hand, limitations of the 1D models may alter the predictions due, for instance, to the lack of a frequency-dependent damping mechanism, along with the disregard of oblique incidence and surface waves, generally not considered in standard 1D wave propagation. Moreover, the choice of a hyperbolic curve to fit the soil degradation and damping curves entails strain localization, due to small values of β close to the surface and to the incapability to attain the real ultimate shear strength. However, the interest of this paper is to assess the seismic response of the KKNPP from a global point of view, instead of studying the exact rheological behaviour of the soil layers: 1D-EQL is still widely used in seismic vulnerability assessment of nuclear power plants, even in extreme strong ground motion earthquake scenarios (IAEA 2014), as well as for the recommendations provided by national seismic codes (such a as the EUROCODE 8, the Japanese building code etc.). The paper stresses some major shortcomings of the model (i.e. the pathological dependence of 1D non-linear seismic analyses on the incident motion direction) and the high level of incertitude in the geotechnical data.

It is clear that the present case of study needs for complex 3D numerical models since complex geology underlies the site, as reported by several authors (Aochi et al. 2013; Tsuda et al. 2011; Gatti 2017). Due to the near-field conditions, the seismological model should also include the faulting mechanism to be able to model the impulsive nature of seismic records.

Acknowledgements This work, within the SINAPS@ project, benefited from French state funding managed by the National Research Agency under program RNSR Future Investments bearing Reference No. ANR-11-RSNR-0022-04. The research reported in this paper has been supported in part by the SEISM Paris Saclay Research Institute. TEPCO (Tokyo Electric Power Company) is gratefully appreciated for disseminating the valuable strong motion records during the 2007 Niigataken Chuetsu-Oki earthquake.

References

Aochi H, Ducellier A, Dupros F, Delatre M, Ulrich T, de Martin F, Yoshimi M (2013) Finite difference simulations of seismic wave propagation for the 2007 Mw 6.6 Niigata-ken Chuetsu-Oki earthquake: validity of models and reliable input ground motion in the near field. Pure Appl Geophys 170(1–2):43–64

Aoi S, Sekiguchi H, Morikawa N, Kunugi T (2014) Source process of the 2007 Niigata-ken Chuetsu-Oki earthquake derived from near-fault strong motion data. Earth Planets Space 60(11):1131–1135

Baker JW (2007) Quantitative classification of near-fault ground motions using wavelet analysis. Bull Seismol Soc Am 97(5):1486–1501

Bolt BA (2004) Seismic input motions for nonlinear structural analysis. ISET J Earthq Technol 41(448):223–232

Building Research Institute, Japan Society of Seismic Isolation, and Kenchiku Kenkyu Shinko Kyokai (2001) Technical background of the provisions of seismically isolated buildings in the revised building standard law of Japan. Gyosei (**in Japanese**)

Cox KE, Ashford SA (2002) Characterization of large velocity pulses for laboratory testing, Technical Report April. Pacific Earthquake Engineering Research Center

Curtis A, Gerstoft P, Sato H, Snieder R, Wapenaar K (2006) Seismic interferometry—turning noise into signal. Lead Edge 25:1082–1092
Darendeli MB (2001) Development of a new family of normalized modulus reduction and material damping curves, Ph.D. thesis. The University of Texas at Austin
Faccioli E, Vanini M (2003) Complex seismic site effects in sediment-filled valleys and implications on design spectra. Prog Struct Mater Eng 5(4):223–238
Gatti F (2017) Forward physics-based analysis of "source-to-site" seismic scenarios for strong ground motion prediction and seismic vulnerability assessment of critical structures, Ph.D. thesis. CentraleSupélec and Politecnico di Milano
Gatti F, Lopez-Caballero F, Clouteau D (2015) One-dimensional seismic soil response at the Nuclear Power Plant of Kashiwazaki-Kariwa during the 2007 Niigata-Chuetsu-Oki earthquake. In Kruis J, Tsompanakis Y, Topping B (eds) Proceedings of the fifteenth international conference on civil, structural and environmental engineering computing, number 157 in Computational, Engineering and Technology Conferences and Publications. Civil-Comp Press, Stirlingshire, pp 1–16
Green R, Cameron WI (2003) The influence of ground motion characteristics on site response coefficients. In: PCEE 2003: 7th Pacific conference on earthquake engineering. New Zealand Society for Earthquake Engineering, pp 1–8
Hartzell S, Bonilla LF, Williams R (2004) Prediction of nonlinear soil effects. Bull Seismol Soc Am 94(5):1609–1629
Hashash YMA, Groholski DRPC (2010) Recent advances in non-linear site response analysis. In: Recent advances in geotechnical earthquake engineering and soil dynamics and symposium in Honor of Professor I.M. Idriss, number OSP 4, pp 1–22
IAEA (2014) Review of seismic evaluation methodologies for nuclear power plants based on a benchmark exercise. International Atomic Energy Agency, Vienna. IAEA-TECDOC-1722
Kaklamanos J, Bradley BA, Thompson EM, Baise LG (2013) Critical parameters affecting bias and variability in site-response analyses using KiK-net downhole array data. Bull Seismol Soc Am 103(3):1733–1749
Kato A, Sakai S, Kurashimo E, Igarashi T, Iidaka T, Hirata N, Iwasaki T, Kanazawa T (2008) Imaging heterogeneous velocity structures and complex aftershock distributions in the source region of the 2007 Niigataken Chuetsu-Oki earthquake by a dense seismic observation. Earth Planets Space 60:1111–1116
Kawase H (2011) Strong motion characteristics and their damage impact to structures during the off Pacific Coast of Tohoku earthquake of March 11, 2011: how extraordinary was this M9.0 earthquake. In: 4th IASPEI-IAEE international symposium-effects of surface geology on seismic motion, vol 11, pp 1–13
Kayen R, Brandenberg SJ, Collins BD, Dickenson S, Ashford S, Kawamata Y, Tanaka Y, Koumoto H, Abrahamson N, Cluff L, Tokimatsu K, Johnson L (2009) Geoengineering and seismological aspects of the Niigata-Ken Chuetsu-Oki Earthquake of 16 July 2007. Earthq Spectra 25(4):777–802
Kokusho T, Suzuki T (2008) Vertical array records during 2007 Niigata-Ken Chuetsu-Oki earthquake and incident wave energy. In: The 14th World conference on earthquake engineering
Kramer SL (1996) Geotechnical earthquake engineering, vol 6. Prentice-Hall, Englewood Cliffs
Kwok AOL, Stewart JP, Hashash YMA, Matasovic N, Pyke R, Wang Z, Yang Z (2007) Use of exact solutions of wave propagation problems to guide implementation of nonlinear seismic ground response analysis procedures. J Geotech Geoenviron Eng 133(11):1385–1398
Luco N, Cornell C (2007) Structure-specific scalar intensity measures for near-source and ordinary earthquake ground motions. Earthq Spectra 23(2):357–392
Mavroeidis G, Papageorgiou A (2003) A mathematical representation of near-fault ground motions. Bull Seismol Soc Am 93(3):1099–1131
Mavroeidis G, Dong G, Papageorgiou A (2004) Near-fault ground motions, and the response of elastic and inelastic single-degree-of-freedom (SDOF) systems. Earthq Eng Struct Dyn 33(9):1023–1049
Menq F-Y (2003) Dynamic properties of sandy and gravelly soils, Ph.D. thesis. The University of Texas at Austin
Ministry of Land, Infrastructure and Transport (2000) Notification No. 2009-2000, Technical Standard for Structural Specifications and Calculation of Seismically Isolated Buildings (**in Japanese**)
Ministry of Land, Infrastructure and Transport, Building Research Institute, Japan Conference of Building Officials, Japan Society of Seismic Isolation, and Building Center of Japan (2001) Commentary on technical standards and calculation procedures of seismically isolated buildings. Kogaku-tosho (**in Japanese**)
Miura K, Kobayashi S, Yoshida N (2000) Equivalent linear analysis considering large strains and frequency dependent characteristics. In: 12th WCEE, pp 1–8

Midorikawa M, Iiba M, Koshika N (2004) Seismic performance evaluation of seismically isolated buildings introduced to the building code of Japan. J Pressure Vessel Technol (ASME) 126:18–24
Mogi H, Shrestha SM, Okamura S, Kawakami H (2010) Nonlinear soil behavior observed at vertical array in the Kashiwazaki-Kariwa Nuclear Power Plant during the 2007 Niigata-ken Chuetsu-Oki earthquake. Bull Seismol Soc Am 100(2):762–775
Nakagawa K, Soga K (1995). Nonlinear cyclic stress–strain relation for soils. In: 3th international conference on recent advances in geotechnical earthquake engineering and soil dynamics
Newmark NM, Hall W (1982) Earthquake design and spectra. In: Agbabian M (ed) Engineering monographs on earthquake criteria, structural design, and strong motion records. The Earthquake Engineering Research Institute, Oakland, p 103
Ozawa T (2008) Coseismic deformation of the 2007 Chuetsu-Oki earthquake derived from PALSAR/InSAR and its fault model. Earth Planets Space 60(11):1099–1104
Pavlenko OV, Irikura K (2012) Nonlinear soil behavior at the Kashiwazaki-Kariwa Nuclear Power Plant during the Niigata Chuetsu-Oki earthquake (July, 16, 2007). Pure Appl Geophys 169(10):1777–1800
Pecker A (2011) Ground response analysis-Kashiwazaki-Kariwa nuclear plant-Unit 7 R/B, Technical report. Geodynamique et Structures
Penzien J, Watabe M (1975) Characteristics of 3-dimensional earthquake ground motions. Earthq Eng Struct Dyn 3(1975):365–373
Rathje EM, Abrahamson NA, Bray JD (1998) Simplified frequency content estimates of earthquake ground motions. J Geotech Geoenviron Eng 91:150–159
Regnier J, Cadet H, Bonilla LF, Bertrand E, Semblat J-F (2013) Assessing nonlinear behavior of soils in seismic site response: statistical analysis on KiK-net strong-motion data. Bull Seismol Soc Am 103(3):1750–1770
Rezaeian S, Der Kiureghian A (2012) Simulation of orthogonal horizontal ground motion components for specified earthquake and site characteristics. Earthq Eng Struct Dyn 41(2):335–353
Spudich P, Bayless J, Baker JW, Chiou B, Rowshandel B, Shahi S, Somerville P (2013) Final Report of the NGA-West2 directivity working group, Technical Report 2013/09. Pacific Earthquake Engineering Research Center, College of Engineering, University of California
TEPCO (2008) The data analysis recorded at the Kashiwazaki Kariwa Nuclear Power Plant during the 2007 Niigata-ken Chuetsu-oki earthquake. Technical Report. The Tokyo Electric Power Company, Inc (**in Japanese**). http://www.tepco.co.jp/cc/press/betu07_j/images/070730d.pdf
Thompson EM, Baise LG, Kayen RE, Guzina BB (2009) Impediments to predicting site response: seismic property estimation and modeling simplifications. Bull Seismol Soc Am 99(5):2927–2949
Tokimatsu K, Arai H (2008) Nonlinear soil properties estimated from downhole array recordings at Kashiwazaki-Kariwa nuclear power plant in the Niigata-Ken Chuetsu-Oki earthquakes. In: The 14th World conference on earthquake engineering. World Conferences on Earthquake Engineering, Beijing, pp 2–9
Tsuda K, Hayakawa T, Uetake T, Hikima K, Tokimitsu R, Nagumo H, Shiba Y (2011) Modeling 3D velocity structure in the fault region of the 2007 Niigataken Chuetu-Oki earthquake with folding structure. In: 4th IASPEI/IAEE international symposium-effects of surface geology on seismic motion, pp 1–11
Uetake T, Nishimura I, Mizutani H (2008) Characteristics of strong motion records in Kashiwazaki-Kariwa Nuclear Power Station during the Niigataken Chuetsu-Oki earthquake in 2007. In: 14th WCEE
Vardanega PJ, Bolton MD (2013) Stiffness of clays and silts: normalizing shear modulus and shear strain. J Geotech Geoenviron Eng 139(9):1575–1589
Wald D, Quitoriano V, Heaton T, Kanamori H (1999) Relationship between peak ground acceleration, peak ground velocity, and modified Mercalli intensity in California. Earthq Spectra 15(3):557–564
Yee E, Stewart J, Tokimatsu K (2011) Nonlinear site response and seismic compression at vertical array strongly shaken by the Niigata-ken Chuetsu-Oki earthquake, Technical report. Pacific Earthquake Engineering Research Center, College of Engineering, University of California, Berkeley